

Facile Synthesis of a Multifunctional SnO₂ Nanoparticles/Nanosheets Composite for Dye-Sensitized Solar Cells

Dongting Wang,* Yuchen Li, Yimin Ding, Xiangchen Jia, Daopeng Zhong, Xianxi Zhang, Jinsheng Zhao, and Yuzhen Fang



Cite This: *ACS Omega* 2023, 8, 44578–44585



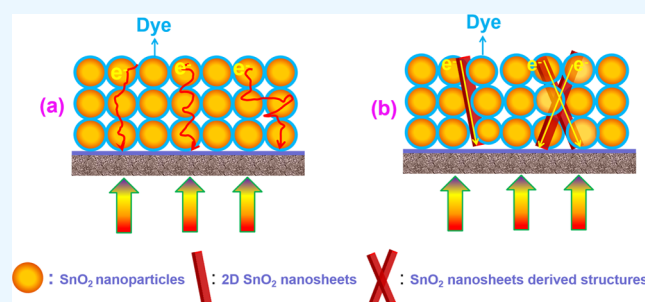
Read Online

ACCESS |

Metrics & More

Article Recommendations

ABSTRACT: Synthesizing SnO₂ composite nanostructures via a facile one-step method has been proven to be a great challenge. By adjusting operating variables, such as the reaction solution's pH and solvent type, several SnO₂ nanostructures, in particular, a function-matching SnO₂ hybrid structure composed of irregular zero-dimensional nanoparticles (NPs) and two-dimensional nanosheets (NSs), could be created. The as-prepared SnO₂ composites were then characterized by X-ray diffraction (XRD), transmission electron microscopy (TEM), scanning electron microscope (SEM), and diffuse reflectance spectroscopy (DRS) to determine their physical properties. Dye-sensitized solar cells (DSCs) constructed with the resultant multifunctional SnO₂ NPs/NSs composite exhibited the highest overall power conversion efficiency (PCE) of 5.16% among all products with a corresponding short-circuit current density of 18.6 mA/cm² and an open-circuit voltage of 0.626 V. The improved performance can be attributed to the combined effects of each component in the composite, i.e., the intentionally introduced nanosheets provide desired electron transport and enhanced light scattering capability, while the nanoparticles retain their large surface area for efficient dye absorption.



1. INTRODUCTION

Dye-sensitized solar cells (DSCs) have attracted tremendous interest over the past decade and have shown significant promise for practical photovoltaic applications owing to their low cost and effective photovoltaic performance.^{1–3} Since the first study on mesoporous titania-based photoanode films was published in 1991, numerous studies on DSCs have been conducted. To date, efficiencies of more than 12% have been achieved by using a mesoporous film of sintered TiO₂ nanoparticles as the photoanode.^{4,5} In addition to the frequently used TiO₂, alternative semiconductors with broad band gaps, such as SnO₂,^{6,7} ZnO,^{8,9} Nb₂O₅,^{10,11} and Zn₂SnO₄,^{12,13} are also being investigated. Among them, SnO₂ is one of the promising and reliable candidates for DSCs due to its wide band gap (3.62 eV) and high electron mobility (100–200 cm² V⁻¹ s⁻¹) compared to TiO₂.^{14–18} Such exceptional features make it favorable for electron transfer within the photoanode film, thereby improving the photo-conversion efficiency of the DSCs. However, charge trapping that occurs at the grain boundaries during charge transport through the disordered SnO₂ nanoparticles (NPs) would inevitably result in the scattering of free electrons and reduction of carrier mobility in the SnO₂ photoanode film.^{19–23} As a promising alternative to zero-dimensional (0D) nanostructures, two-dimensional (2D) nanosheets are of

particular interest in performance enhancement for DSCs, since the nanostructures favor electron transport through direct pathways.^{24–28} However, the efficiency of 2D SnO₂ nanostructures is still relatively low because the improved electron transport characteristic is never large enough to offset the impact of the sacrificed accessible surface area. Indeed, it is challenging to produce a highly efficient photoanode with a single morphology and/or component, since it is hard to simultaneously integrate the required prerequisites, i.e., high specific surface area, outstanding light scattering, and fast electron transport qualities.

The combination of various monodimensional nanostructures offers a greater chance to assemble all of the required favorable characteristics, hence making it possible for improving the efficiency of DSCs. To date, some novel composite architectures have been synthesized and applied as photoanodes in DSCs. For example, Xing et al. developed a composite photoanode consisting of 0D TiO₂ nanoparticles

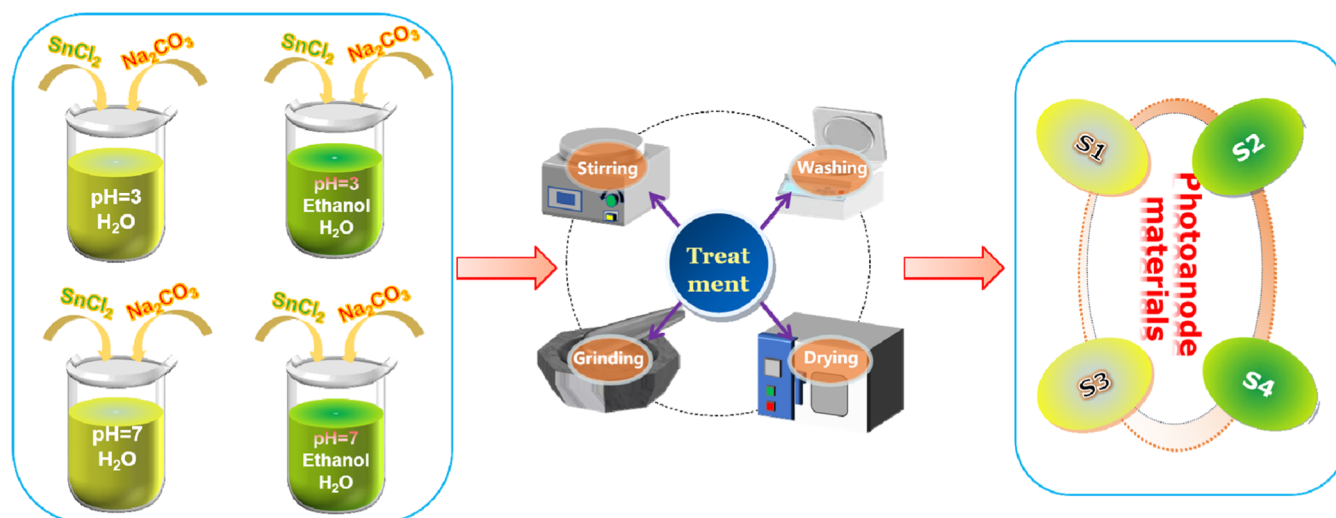
Received: June 23, 2023

Revised: October 31, 2023

Accepted: November 1, 2023

Published: November 15, 2023



Scheme 1. Schematic Illustration for the Synthesis of Various SnO₂ Photoanode Materials

and 2D SnO₂ nanosheets, in which SnO₂ nanosheets effectively accelerated charge transport and improved light scattering, thus showing more than 2 times higher efficiency than that of DSCs based on conventional SnO₂ nanoparticles.²⁹ In addition, Yang et al. integrated 2D SnO₂ nanosheets into TiO₂-based photoanodes and discovered that in this system, the 2D scaffolds could not only promote the transport of photogenerated electrons across the film but also significantly enhance the light scattering property of the photoanode.³⁰ The aforementioned studies not only demonstrated the beneficial effects of the introduced component on promoting the efficiency of the resulting cells but also strengthened the understanding of the composite photoanode. However, it should be noted that the majority of studies have been concentrated on the combination of SnO₂ with other semiconductor oxides, and little attention has been paid to SnO₂ composite architectures, especially 0D/2D composites. On the other hand, the construction of composite photoanodes is always subjected to a multistep process, in which the used nanostructures are generally synthesized separately, followed by mixing them together via certain techniques. These methods not only make the synthesis procedure complicated but also increase the cost of the preparation process.^{31,32} In this regard, preparing the SnO₂ composite structures through a more facile approach as opposed to the common one-by-one strategy is urgently desirable, which has yet to be reported.

Here, the 2D SnO₂ NSs and 0D SnO₂ NPs composite are intentionally designed via a facile one-step method based on the morphology and structure matching strategy, within which 2D SnO₂ NSs act as charge transport pathways for accelerated electron transport within the film and light scattering center for efficient light utilization, while disordered 0D SnO₂ NPs play the vital role of offering the accessible surface area for sufficient dye uptake. One key feature of our study is fabricating SnO₂ NPs/NSs composites via a simple one-step method achieved by finely tuning the operation conditions (i.e., pH values and solvent types). The resulting SnO₂ NP/NS composite architecture was used to fabricate DSCs, and an improved overall efficiency of 5.16% was obtained, showing a significant 36.1% increase over the cell constructed with SnO₂ NPs. Various analyses demonstrated that the following advantageous

properties, including fast charge transport, large dye uptake, and strong light scattering capability, derived from the synergistic effects of both components contributed to the enhanced photovoltaic performance of such an innovative SnO₂ composite photoanode, indicating the promise of the composite nanostructure for the further improvement of DSCs.

2. EXPERIMENTAL SECTION

2.1. Materials. *tert*-Butylpyridine (*t*-BPy), lithium iodide (LiI), 2,3-dimethyl-1-propyl imidazolium iodide (DMPII), iodide (I₂), 3-methoxypropionitrile, and acetonitrile were the beginning electrolyte ingredients, and they were all purchased from Sigma. Analytical grade substances, including SnCl₂·2H₂O, H₂PtCl₆, Na₂CO₃, TiCl₄, H₂O₂, and ethanol, were all utilized without additional purification. The ruthenium-based dye N719 used in the study was obtained from Solaronix (Aubonne, Switzerland). As a conductive transparent electrode, F-doped tin oxide (FTO) glass was obtained from Nippon, Japan (7 Ω/sq, 84% transmittance).

2.2. Preparation of SnO₂. SnO₂ was prepared by hydrolyzing the Sn precursor, SnCl₂, at room temperature while regulating the pH levels and the kind of solvent. Taking the SnO₂ NSs/NPs composite as a sample (labeled as S2), a 40 mL mixed solution of water and ethanol (1:1, v/v) with a preadjusted pH value of 3 (regulated by adding a certain amount of 0.01 M HCl) was initially prepared. 2.256 g of SnCl₂·2H₂O was then added to the above solution, followed by the addition of 1.06 g of Na₂CO₃ under magnetic stirring. After that, the white suspension was continuously stirred at room temperature for 4 h. The resultant colloidal suspension was washed with deionized water 5 times by centrifugation at a rate of 4000 rpm for 10 min to remove the impurities. The harvested product was subsequently dried at 60 °C in air for 6 h. Following the aforementioned process, another sample, designated as S1, was synthesized under identical conditions but with water as the solvent. Similarly, the photoanode materials prepared under other conditions, namely, pH = 7 with both water and water/ethanol (1:1, v/v) as solvents, were also generated and named S1 and S3, respectively (see Scheme 1).

2.3. SnO₂ Photoelectrode Preparation and Solar Cell Fabrication. FTO conducting glass was utilized as the substrate for various SnO₂ photoelectrodes. Before electrode fabrication, the FTO substrates were progressively cleaned in HCl, acetone, ethanol, and water for 15 min each in an ultrasonic bath. A viscous SnO₂ paste was prepared by grounding SnO₂ (0.2 g) for 40 min in a mixture of ethanol (2 mL), terpineol (0.6 g), and ethyl cellulose (0.1 g), which was then sequentially coated on the FTO substrate using the doctor-blading technique. After drying at 80 °C for 2 h, the SnO₂ photoanode was heated in a programmed procedure (i.e., at 325 °C for 5 min first, then at 375 °C for 5 min, followed by at 450 °C for 15 min, and finally at 500 °C for 15 min). Coating TiO₂ on the surface of SnO₂ was first performed by immersing the as-prepared SnO₂ electrodes in an aqueous solution of TiCl₄ at a concentration of 40 mM at 80 °C for 30 min. Then, the photoanode was washed with distilled water and ethanol to remove residual TiCl₄, followed by sintering at 500 °C for 60 min at a heating rate of 5 °C min⁻¹. In the present study, to maintain the same film thickness, the adhesive tape layers and SnO₂ paste used in film preparation are strictly controlled. After cooling, SnO₂ electrodes with an active area of 0.16 cm² (0.4 cm × 0.4 cm) were designated and immersed in a 0.5 mM N719 dye solution in absolute ethanol for 24 h at room temperature. The dye-sensitized SnO₂ photoanode and a Pt counter electrode were then sealed by a thermoplastic sealant to make a face-to-face cell. Finally, an electrolyte solution made of 1.0 M DMPII, 0.12 M I₂, 0.1 M LiI, and 0.5 M *t*-BPy in 3-methoxypropionitrile was injected into the specified space.

2.4. Material Characterization and Photoelectrochemical Measurements. The crystal structures of the as-synthesized SnO₂ powder were characterized using an X-ray diffractometer (X'Pert PRO MPD, PANalytical, Almelo, the Netherlands). The morphologies of the resulting products were determined by a transmission electron microscope (TEM, Talos F200X) and a scanning electron microscope (SEM, JEOL-6701F, FEI). The dye loading in the SnO₂ electrode was examined first by desorbing dye molecules from the sensitized photoanode film (1 × 1 cm²) into a 1.0 M NaOH solution (water/ethanol, 50:50 (v/v)), followed by detecting its concentration via a UV-vis spectrophotometer (Lambda 950, PerkinElmer). Nitrogen adsorption-desorption isotherms were acquired from an Autosorb iQ-XR surface area analyzer (Quantachrome Instruments). The photocurrent density-voltage characteristics were measured on an electrochemical workstation (CHI760, Shanghai) under simulated AM 1.5 sunlight illumination with 100 mW cm⁻² light output. Electrochemical impedance spectroscopy (EIS) measurements of the constructed cells were performed on an electrochemical workstation (CHI760, CH Instruments) at an applied bias of 0.55 V and a frequency range from 0 Hz to 10⁵ Hz with a fixed ac amplitude of 10 mV.

3. RESULTS AND DISCUSSION

3.1. XRD Analysis. The typical X-ray diffraction (XRD) patterns of the as-prepared SnO₂ samples are shown in Figure 1a. As can be observed, all of the resolved diffraction peaks are without a doubt associated with the cassiterite structure (JCPDS No. 41-1445), and no peaks associated with any other samples are discovered, proving that low-valence Sn (Sn²⁺) are converted to SnO₂ during the stirring process. This outcome is in line with our most recent study, in which SnO₂

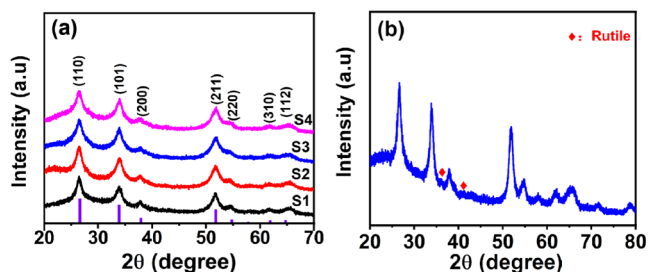


Figure 1. XRD patterns of (a) the as-synthesized SnO₂ powder samples and (b) the resultant photoanode film. Vertical bars with purple colors below the patterns represent the standard diffraction data from JCPDS files for tetragonal cassiterite (SnO₂).

aggregates were created at room temperature utilizing SnCl₂ as a precursor.^{33,34} Moreover, it can be seen from Figure 1a that materials S1–S4 exhibit nearly identical peak intensities, suggesting that the solvent and pH have a negligible effect on the crystallinity of SnO₂ products. Using Scherrer's formula ($d = 0.9\lambda/\beta \cos \theta$), the average crystallite size was calculated from the full width at half-maximum (fwhm) of the (110) peak and ranges between 5 and 6 nm. For the case of TiCl₄-treated SnO₂ (S2), additional XRD peaks corresponding to rutile TiO₂ (JCPDS No. 21-1272, Figure 1b) also appear at $2\theta = 36.09$ and 41.22° in addition to the SnO₂ structure, confirming the existence of TiO₂ nanocrystallites on the surface of the SnO₂ film.² It is anticipated that the TiO₂ coating will have a substantial effect on the chemical and photoelectrochemical properties of SnO₂, leading to better dye absorption and injection efficiency of photogenerated electrons into semiconductors, thereby increasing the photoelectric conversion efficiency.

3.2. Morphology and Structure Characterization of the SnO₂ Composite. For the optimization of the SnO₂ photoanode materials, the impact of pH and the kind of solvent is investigated. From the low-magnification transmission electron microscopy (TEM) image (Figure 2a), it can be obviously seen that product S1 is made of disordered nanostructures composed of small interconnected nanoparticles. Surprisingly, it is discovered that switching from water to a solvent mixture of water and ethanol has a significant impact on the shape of the product (S2) under the same acidic setting (pH 3), resulting in the presence of nanosheet structures made up of small crystals (see Figure 2b,c). This morphology variation could be related to the dielectric constant of the solvent, which differs greatly between water and the mixture of ethanol–water.³⁵ It is anticipated that the 2D SnO₂ nanosheet structure will lead to significantly enhanced light scattering capability and improved charge transport property, increasing the efficiency of light harvesting and electron collecting. Apart from the type of solvent, the pH of the solution is another synthetic parameter that influences the morphology of the products. As shown in Figure 2d, sample S3 shows a morphology similar to that of sample S1 when the pH value is increased from 3 to 7. This result shows that the pH has a negligible impact on the shape of the as-prepared SnO₂ products when water is used as the fixed solvent. However, at pH 7, the addition of ethanol to the synthetic mixtures (water/ethanol = 1:1) leads to the formation of product S4, which typically consists of aggregates and disordered nanoparticles, with the former making up the vast majority (Figure 2e). According to the systematical

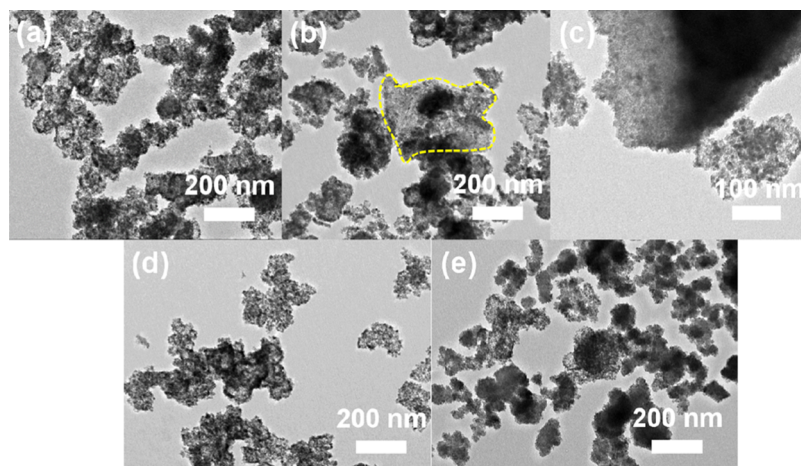


Figure 2. TEM images of S1 (a) and S2 (b) (the inserted yellow circles indicate the sheet structures). (c) TEM image of the nanosheet structure in S2. TEM images of S3 (d) and S4 (e).

investigation, a conclusion can be drawn that pH has an invisible effect on the morphology feature when water is used as the solvent, since only disordered nanoparticles can be obtained in this condition. In contrast, the products produced using a mixture of water and ethanol as a solvent are either aggregates/nanoparticles or nanosheets/nanoparticles composites, depending on the pH levels.

The S2 sample was coated on the FTO substrate using a typical doctor-blade technique followed by annealing and TiCl_4 treatment to create the final photoanode film. Top-view SEM images shown in Figure 3a,b reveal that after TiCl_4

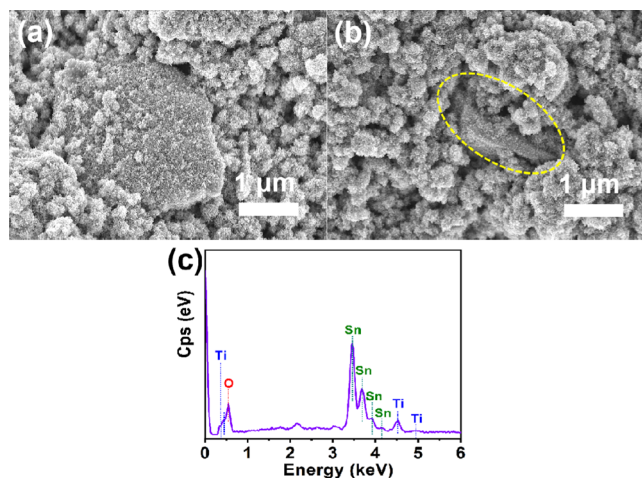


Figure 3. (a, b) SEM images of the obtained films based on sample S2 after being treated with TiCl_4 , and (c) the corresponding EDS spectrum of sample S2 treated with TiCl_4 .

treatment, the S2-based film spreads uniformly over the FTO substrate with a surface structure free of cracks. Besides the random aggregate-like nanostructures, sheet-like morphology could also be clearly seen in the S2 sample-based film, which is consistent with the result displayed in Figure 2b. Moreover, partially oriented sheets are also observed to be entwined among the SnO_2 aggregates, demonstrating retention of the specific nanostructures in the photoanode films. This characteristic is greatly desired, since the beneficial orientation offers direct paths for fast electron transport within the resulting photoanode film.^{36,37} The energy-dispersive spectro-

scopy (EDS) spectrum (Figure 3c), consisting of Sn, O, and Ti peaks, demonstrates the existence of SnO_2 and the successful coating of TiO_2 on the as-prepared SnO_2 photoanode film.

3.3. Photovoltaic Performance. The current density versus voltage (J - V) curves of the solar cells based on photoelectrode films constructed with various SnO_2 nanostructures were recorded under AM 1.5 illumination (100 mW cm^{-2}) to examine the photoelectric conversion efficiency (PCE). The typical J - V curves of several SnO_2 photoelectrode films are shown in Figure 4, and the details of the calculated

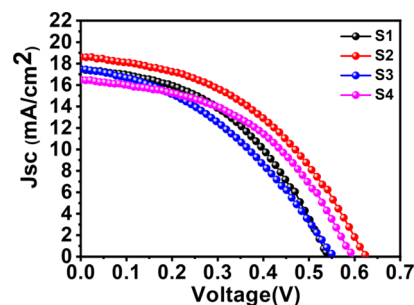


Figure 4. J - V curves of DSCs fabricated with the four SnO_2 samples.

photovoltaic parameters are gathered in Table 1. As observed, the S1-based cell only exhibited a PCE of 4.38% with a short-circuit current (J_{SC}) of 17.5 mA cm^{-2} and an open-circuit voltage of 0.539 V. In contrast, when the solvent is switched from water to a solution of water and ethanol, the J_{SC} and V_{OC} increase to 18.6 mA cm^{-2} and 0.626 V, respectively, yielding an excellent conversion efficiency of 5.16%. Apparently, the photovoltaic characteristics listed above are substantially better than those of S1. The superior photovoltaic performance, we believe, is primarily associated with the distinctive structure of sample S2, which contains the desired nanosheets created during the reaction process as a result of the addition of ethanol to the solvent. Moreover, the phenomenon is consistent with previous reports on various photoanode composites based on other metal oxide nanosheets, indicating the same effect that the sheet structure should permit or at least facilitate the advancement of the DSCs device performance.^{38–40} The photovoltaic performance of samples S3 and S4 shows some falloff in comparison with S2. In particular, the J_{SC} falls to 17.5 and 16.5 mA cm^{-2} along with the drop of V_{OC} to

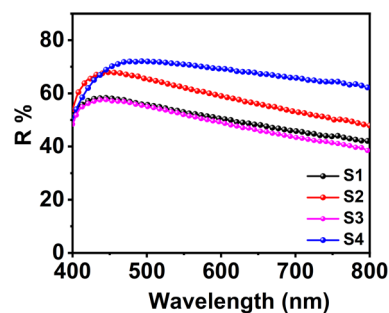
Table 1. Characteristics of Different SnO₂ Photoelectrodes and the Corresponding Photovoltaic Parameters (J_{sc} , V_{oc} , FF, and PCE) of DSCs

sample	J_{sc} (mA/cm ²)	V_{oc} (V)	FF	PCE	S_{BET} (m ² /g)	adsorbed dye ($\times 10^{-7}$ mol/cm ²)	R_{ct} (Ω)
S1	17.5	0.539	45.3	4.28	45.5	1.63	19.6
S2	18.6	0.626	44.3	5.16	51.4	1.75	12.2
S3	17.5	0.552	39.2	3.79	43.2	1.56	23.2
S4	16.5	0.594	46.8	4.59	44.5	1.61	16.1

0.552 and 0.594 V, thus leading to inferior photoelectric performances of 3.79 and 4.59%, respectively. Evidently, the devices' efficiencies of the samples synthesized at pH 3 are much higher than that of the corresponding samples produced at pH 7. Moreover, it can be interestingly discovered that the SnO₂ composite has a notable advantage over the nanoparticles that are irregularly packed. Regarding S2 and S4, considering that they both consist of two structures, the differences in performance between the two samples may result from the distinct effects of the incorporated unique structures, such as nanosheets and aggregates, on the associated cells. For a thorough explanation of the performance variance, the dye loading capacity, light harvesting efficiency, and electron transport properties of all cells will be experimentally investigated.

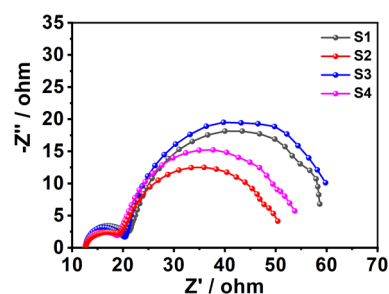
3.4. Dye Loading Amount and Reflectance Spectra Measurements. To reveal the underlying causes for the distinct photovoltaic behaviors of the SnO₂-based cells, the characterization of dye loading amounts into the four different photoanode films was first carried out by measuring the concentration of the dye desorbed from SnO₂ films using UV–vis absorption spectroscopy, and the result is listed in Table 1. Obviously, compared with the sample S1-based film (1.63×10^{-7} mol/cm²), the composite S2-based film exhibits much better ability in dye uptake with the loading amount reaching 1.75×10^{-7} mol/cm². Given that the production method and thickness of the photoanode films are identical, the dye loading improvement is most likely connected to the morphological variation-derived increase in the overall surface area. The above speculation is well-supported by the Brunauer–Emmett–Teller (BET) data as presented in Table 1, in which the S_{BET} of S2 (51.4 m²/g) increases to some extent in comparison with that of S1 (45.5 m²/g). A large dye loading amount of the film enables the incident photons to be absorbed sufficiently, thus giving rise to a high overall efficiency. For S4, even though the resultant film displays a better dye absorption capacity than S3, the dye loading amount is still lower than that of S2. This could be due to the coalescence of nanocrystals in the aggregates, which thus limits the dye absorption to a low level.

UV–vis reflectance spectroscopy was recorded (see Figure 5) to assess the light-trapping properties of the four samples. Notably, in contrast to S1 and S3, S2 and S4 exhibit more vital light-reflecting abilities throughout a wide wavelength range (400–800 nm). In other words, samples composed of a SnO₂ composite have better scattering properties than SnO₂ NPs-only products. This makes sense given that the hierarchical structures in this study, namely, SnO₂ nanosheets and aggregates, can serve as light scattering centers, increasing the likelihood of photons being absorbed by the sensitizer molecules owing to the multiple reflection and scattering. On the other aspect, it should be pointed out that S4 exhibits even higher scattering capability than S2 in the whole wavelength range. It is reported that both nanosheets and agglomerates

**Figure 5.** Diffuse reflectance spectra of all four SnO₂ films.

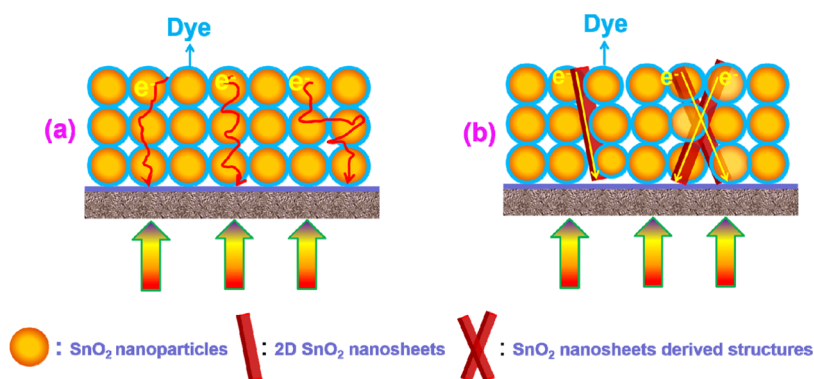
have discernible light scattering properties, which is also consistent with the results of our testing.^{33,41,42} The above difference may imply that the agglomerates in the sample have a much stronger light scattering capability than the nanosheets. As for the reflectance discrepancy between S3 and S4, this is also understandable because sample S4 possesses a large number of aggregates, while S3 only consists of disordered nanoparticles with much weaker light scattering ability.

3.5. EIS Analysis. To reveal and deeply understand the difference in the internal interfacial recombination reactions of the photoexcited electrons in DSCs, we performed EIS measurements under a simulated solar light of 100 mW/cm². Figure 6 illustrates the Nyquist plots of all four devices from S1

**Figure 6.** Nyquist plots of DSCs based on S1–S4.

to S4. It can be seen that the Nyquist plots spectra of all samples exhibit two well-defined semicircles in the frequency regions of >1 kHz and 100–1 Hz, which correspond to the electrochemical reactions that occur at the Pt counter electrode and the SnO₂ film/dye/electrolyte interface, respectively.^{43,44} As the resistances of the electrochemical reactions are the same, the difference in charge recombination resistance is mostly governed by the extent of electron transport in the photoanode, which could be determined by the diameter of the right semicircle. As shown in Figure 6, an apparent increasing trend of the central arc diameter in the order of S3 > S1 > S4 > S2 is observed; therefore, it can be deduced that the interfacial charge recombination resistance for the S2-based DSCs gets significantly suppressed by modulating the morphology of the composite. According to

Scheme 2. Schematic Illustration of Possible Electron (e^-) Diffuse Transport in the (a) SnO_2 Nanoparticle Photoanode Film with an Irregular Morphology and (b) SnO_2 NPs/NSs Composite Photoanode Film



the fitted values of R_{ct} listed in Table 1, it can be seen that R_{ct} decreases dramatically from 19.6 Ω for the S1-based cell to 12.2 Ω for the S2-based cell with the introduction of NS, implying slower electron recombination for the SnO_2 NP/NS films. This observation is explainable, since the injected electrons are prone to recombine with I_3^- in the electrolyte for the disordered nanoparticle-based film (S1) before reaching the collector electrode because the trap defects and structural disorders at the boundaries between nanoparticles will result in reduced carrier mobility due to the free electron scattering.^{45,46} However, after introducing SnO_2 NSs (i.e., S2), the electron generated could be able to travel through the photoanode film more readily because of the advantageous electron transport route created by the SnO_2 NSs (see Scheme 2), which promoted electron diffusion and collection efficiency. Moreover, as reported in the work of other groups, charge recombination also has a crucial influence on the V_{oc} of DSCs.^{47,48} Therefore, the aforementioned higher V_{oc} for S2 could be attributed to decreased charge recombination in the conduction band of SnO_2 . As for S4, it can be seen that the value of R_{ct} is increased to 16.1 Ω , which demonstrates that compared with the partial zigzag pathway for the electron transfer transport route arising from SnO_2 aggregates, the electron transfer along the SnO_2 NSs is more favorable, which fully proves the vital role of the SnO_2 NSs in promoting electron transport.

4. CONCLUSIONS

In summary, several SnO_2 nanostructures, in particular a function-matching SnO_2 hybrid structure made up of disordered 0D SnO_2 NPs and SnO_2 NSs architectures, were designed based on a simple one-step method by finely modulating operating conditions. The investigation into photovoltaic performance showed that the type of solvent and pH had a significant impact on the properties of SnO_2 -based photoanodes, and the desirable SnO_2 NPs/NSs composite synthesized at pH = 3 with water/ethanol as the solvent demonstrated the highest power conversion efficiency of 5.16% with a J_{sc} value of 18.6 mA cm^{-2} and a V_{oc} value of 0.626 V. A variety of materials and device characterization demonstrated that the high dye loading amount, favorable electron transport property, and moderate light scattering capability induced by 2D NSs contributed to the efficient PCE. The aforementioned findings demonstrated that SnO_2 NPs/NSs might be a promising photoanode material for highly efficient DSCs.

AUTHOR INFORMATION

Corresponding Author

Dongting Wang – Shandong Provincial Key Laboratory of Chemical Energy Storage and Novel Cell Technology, School of Chemistry and Chemical Engineering, Liaocheng University, Liaocheng 252059, China; orcid.org/0000-0002-5350-6027; Phone: +86 635 8230647; Email: wtdcell@126.com; Fax: +86 635 8239001

Authors

Yuchen Li – Shandong Provincial Key Laboratory of Chemical Energy Storage and Novel Cell Technology, School of Chemistry and Chemical Engineering, Liaocheng University, Liaocheng 252059, China

Yimin Ding – Shandong Provincial Key Laboratory of Chemical Energy Storage and Novel Cell Technology, School of Chemistry and Chemical Engineering, Liaocheng University, Liaocheng 252059, China

Xiangchen Jia – Shandong Provincial Key Laboratory of Chemical Energy Storage and Novel Cell Technology, School of Chemistry and Chemical Engineering, Liaocheng University, Liaocheng 252059, China

Daopeng Zhong – Shandong Provincial Key Laboratory of Chemical Energy Storage and Novel Cell Technology, School of Chemistry and Chemical Engineering, Liaocheng University, Liaocheng 252059, China

Xianxi Zhang – Shandong Provincial Key Laboratory of Chemical Energy Storage and Novel Cell Technology, School of Chemistry and Chemical Engineering, Liaocheng University, Liaocheng 252059, China

Jinsheng Zhao – Shandong Provincial Key Laboratory of Chemical Energy Storage and Novel Cell Technology, School of Chemistry and Chemical Engineering, Liaocheng University, Liaocheng 252059, China; orcid.org/0000-0002-1576-7971

Yuzhen Fang – Shandong Provincial Key Laboratory of Chemical Energy Storage and Novel Cell Technology, School of Chemistry and Chemical Engineering, Liaocheng University, Liaocheng 252059, China; Present Address: School of Energy and Chemical Engineering, Tianjin Ren'ai College, Tianjin 301636, China

Complete contact information is available at: <https://pubs.acs.org/10.1021/acsomega.3c04472>

Notes

The authors declare no competing financial interest.

ACKNOWLEDGMENTS

This work was supported by the Shandong Province Natural Science Foundation of China (ZR2018LB032) and the Tianjin Education Commission Scientific Research Project (2022KJ046).

REFERENCES

- (1) Ren, Y. M.; Zhang, D.; Suo, J. J.; Cao, Y. M.; Eickemeyer, F. T.; Vlachopoulos, N.; Zakeeruddin, S. M.; Hagfeldt, A.; Grätzel, M. Hydroxamic acid pre-adsorption raises the efficiency of cosensitized solar cells. *Nature* **2023**, *613*, 60–65.
- (2) Wang, D. T.; Hu, Y. F.; Li, Y. C.; Jia, X. C.; Fang, Y. Z.; Zhang, Z. L.; Zhang, X. X. Self-Seeding Synthesis of Hierarchically Branched Rutile TiO₂ for High-Efficiency Dye-Sensitized Solar Cells. *ACS Omega* **2023**, *8* (11), 9843–9853.
- (3) Venkatesan, S.; Chiang, C. Y.; Teng, H.; Lee, Y. L. Monolithic quasi-solid-state dye sensitized solar cells prepared entirely by printing processes. *ACS Sustainable Chem. Eng.* **2023**, *11*, 5293–5302.
- (4) Brian, O'R.; Michäel, G. A. low-cost, high-efficiency solar cell based on dye-sensitized colloidal TiO₂ films. *Nature* **1991**, *353*, 737–740.
- (5) Yella, A.; Lee, H. W.; Tsao, H. N.; Yi, C.; Chandiran, A. K.; Nazeeruddin, M. K.; Diao, E. W. G.; Yeh, C. Y.; Zakeeruddin, S. M.; Graetzel, M. Porphyrin-sensitized solar cells with cobalt (II/III)-based redox electrolyte exceed 12% efficiency. *Science* **2011**, *334*, 629–634.
- (6) DiMarco, B. N.; Sampaio, R. N.; James, E. M.; Barr, T. J.; Bennett, M. T.; Meyer, G. J. Efficiency considerations for SnO₂-based dye-sensitized solar cells. *ACS Appl. Mater. Interfaces* **2020**, *12*, 23923–23930.
- (7) Dissanayake, M.; Umair, K.; Senadeera, G.; Jaseetharan, T.; Weerasinghe, A.; Wijayasinghe, H. Plasmonic gold nanoparticle incorporated mgo-coated SnO₂ photoanode for efficiency enhancement in dye-sensitized solar cells. *Sol. Energy* **2022**, *233*, 363–377.
- (8) Wang, D. T.; Wang, W. X.; Ma, X. Y.; Zhang, C.; Zhao, J. S.; Zhang, X. X. Comparative study on the influence of TiO₂ precursors on ZnO-based dye-sensitized solar cells. *Ind. Eng. Chem. Res.* **2015**, *54*, 12639–12645.
- (9) Ringleb, A.; Klement, P.; Schrmann, J.; Chatterjee, S.; Schlettwein, D. Harnessing the potential of porous ZnO photoanodes in dye-sensitized solar cells by atomic layer deposition of Mg-doped ZnO. *ACS Appl. Energy Mater.* **2022**, *5* (12), 14825–14835.
- (10) Zhang, H. M.; Wang, Y.; Liu, P.; Chou, S. L.; Wang, J. Z.; Liu, H. W.; Wang, G. Z.; Zhao, H. J. Highly ordered single crystalline nanowire array assembled three-dimensional Nb₃O₇(OH) and Nb₂O₅ superstructures for energy storage and conversion applications. *ACS Nano* **2016**, *10*, 507–551.
- (11) Le Viet, A.; Jose, R.; Reddy, M. V.; Chowdari, V. R.; Ramakrishna, S. Nb₂O₅ photoelectrodes for dye-sensitized solar cells: choice of the polymorph. *J. Phys. Chem. C* **2010**, *114*, 21795–21800.
- (12) Saadat, F.; Alizadeh, A.; Roudgar-Amoli, M.; Shariatnia, Z. Exploring the influence of Zn₂SnO₄/ZIF-8 nanocomposite photoelectrodes on boosting efficiency of dye sensitized solar cells. *Ceram. Int.* **2022**, *48*, 21812–21823.
- (13) Ramanathan, R.; Zinigrad, M.; Kasinathan, D.; Poobalan, R. M. Zinc Stannate (Zn₂SnO₄)-based hybrid composite photoanode for dye-sensitized solar cell application. *ACS Appl. Energy Mater.* **2022**, *5*, 11506–11516.
- (14) Wang, Z.; Luan, D.; Boey, F. Y. C.; Lou, X. W. Fast formation of SnO₂ nanoboxes with enhanced lithium storage capability. *J. Am. Chem. Soc.* **2011**, *133*, 4738–4741.
- (15) Mohamed, I. M. A.; Dao, V. D.; Yasin, A. S.; Choi, H. S.; Barakat, N. A. M. Synthesis of novel SnO₂@TiO₂ nanofibers as an efficient photoanode of dye-sensitized solar cells. *Int. J. Hydrogen Energy* **2016**, *41*, 10578–10589.
- (16) Zhao, P. L.; Li, D.; Yao, S. T.; Zhang, Y. Q.; Liu, F. M.; Sun, P.; Chuai, X. H.; Gao, Y.; Lu, G. Y. Design of Ag@C@SnO₂@TiO₂ yolk-shell nanospheres with enhanced photoelectric properties for dye sensitized solar cells. *J. Power Sources* **2016**, *318*, 49–56.
- (17) Souza, A. P. S.; Oliveira, F. G. S.; Nunes, V. F.; Lima, F. M.; Almeida, A. F. L.; de Carvalho, I. M. M.; Graça, M. P. F.; Freire, F. N. A. High performance SnO₂ pure photoelectrode in dye-sensitized solar cells achieved via electrophoretic technique. *Sol. Energy* **2020**, *211*, 312–323.
- (18) Wang, Y. F.; Li, X. F.; Li, D. J.; Sun, Y. W.; Zhang, X. X. Controllable synthesis of hierarchical SnO₂ microspheres for dye-sensitized solar cells. *J. Power Sources* **2015**, *280*, 476–482.
- (19) Dissanayake, M. A. K. L.; Kumari, J. M. K. W.; Senadeera, G. K. R.; Anwar, H. Low cost, platinum free counter electrode with reduced graphene oxide and polyaniline embedded SnO₂ for efficient dye sensitized solar cells. *Sol. Energy* **2021**, *230*, 151–165.
- (20) Dissanayake, M. A. K. L.; Umair, K.; Senadeera, G. K. R.; Jaseetharan, T.; Weerasinghe, A. M. J. S.; Wijayasinghe, H. W. M. A. C. Plasmonic gold nanoparticle incorporated MgO-coated SnO₂ photoanode for efficiency enhancement in dye-sensitized solar cells. *Sol. Energy* **2022**, *233*, 363–377.
- (21) Qian, J. F.; Liu, P.; Xiao, Y.; Jiang, Y.; Cao, Y. L.; Ai, X. P.; Yang, H. X. TiO₂-coated multilayered SnO₂ hollow microspheres for dye sensitized solar cells. *Adv. Mater.* **2009**, *21*, 3663–3667.
- (22) Thapa, A.; Zai, J. T.; Elbohy, H.; Poudel, P.; Adhikari, N.; Qian, X. F.; Qiao, Q. Q. TiO₂ coated urchin-like SnO₂ microspheres for efficient dye-sensitized solar cells. *Nano Res.* **2014**, *7*, 1154–1163.
- (23) Wali, Q.; Fakharuddin, A.; Ahmed, I.; Rahim, M. H. A.; Ismail, J.; Jose, R. Multiporous nanofibers of SnO₂ by electrospinning for high efficiency dye-sensitized solar cells. *J. Mater. Chem. A* **2014**, *2*, 17427–17434.
- (24) Hezam, M.; Alsubaie, M. Q.; Algarni, A.; Ghaithan, H.; Labis, J.; Alduraibi, M. ZnO Nanosheet-Nanowire morphology tuning for Dye-sensitized solar cell applications. *Chem. Phys. Lett.* **2021**, *780*, No. 138953.
- (25) Dharamalingam, K.; Kumar, B. A.; Ramalingam, G.; Florence, S. S.; Raju, K.; Kumar, P. S.; Govindaraju, S.; Thangavel, E. The role of sodium dodecyl sulfate mediated hydrothermal synthesis of MoS₂ nanosheets for photocatalytic dye degradation and dye-sensitized solar cell application. *Chemosphere* **2022**, *294*, No. 133725.
- (26) Bu, I. Y. Y. Novel ZnO decorated SnO₂ nanosheet for dye sensitized solar cell applications. *Optik* **2018**, *157*, 406–409.
- (27) Lin, C. Y.; Lai, Y. H.; Chen, H. W.; Chen, J. G.; Kung, C. W.; Vittala, R.; Ho, K. C. Highly efficient dye-sensitized solar cell with a ZnO nanosheet-based photoanode. *Energy Environ. Sci.* **2011**, *4*, 3448–3455.
- (28) Jiang, L.; Sun, L.; Yang, D.; Zhang, J.; Li, Y. J.; Zou, K.; Deng, W. Q. Niobium-doped (001)-dominated anatase TiO₂ nanosheets as photoelectrode for efficient dye-sensitized solar cells. *ACS Appl. Mater. Interfaces* **2017**, *9*, 9576–9583.
- (29) Xing, J.; Fang, W. Q.; Li, Z.; Yang, H. G. TiO₂-coated ultrathin SnO₂ nanosheets used as photoanodes for dye-sensitized solar cells with high efficiency. *Ind. Eng. Chem. Res.* **2012**, *51*, 4247–4253.
- (30) Yang, S.; Hou, Y.; Xing, J.; Zhang, B.; Tian, F.; Yang, X. H.; Yang, H. G. Ultrathin SnO₂ scaffolds for TiO₂-based Heterojunction Photoanodes in Dye-Sensitized Solar Cells: Oriented Charge Transport and Improved Light Scattering. *Chem. - Eur. J.* **2013**, *19*, 9366–9370.
- (31) Wei, K.; Gu, X. Y.; Chen, E. Z.; Wang, Y. Q.; Dai, Z.; Zhu, Z. R.; Kang, S. Q.; Wang, A. C.; Gao, X. P.; Sun, G. Z.; Pan, X. J.; Zhou, J. Y.; Xie, E. Q. Dissymmetric interface design of SnO₂/TiO₂ side-by-side bi-component nanofibers as photoanodes for dye sensitized solar cells: Facilitated electron transport and enhanced carrier separation. *J. Colloid Interface Sci.* **2021**, *583*, 24–32.
- (32) Wang, Y. L.; Ma, C.; Wang, C.; Cheng, P. F.; Xu, L. P.; Lv, L.; Zhang, H. Design of SnO₂@Air@TiO₂ hierarchical urchin-like double-hollow nanospheres for high performance dye-sensitized solar cells. *Sol. Energy* **2019**, *189*, 412–420.
- (33) Wang, D. T.; Liu, S. H.; Shao, M. F.; Li, Q. Y.; Gu, Y. K.; Zhao, J.; Zhang, X. X.; Zhao, J. S.; Fang, Y. Z. Aqueous Solution-Processed

Multifunctional SnO₂ Aggregates for Highly Efficient Dye-Sensitized Solar Cells. *Ind. Eng. Chem. Res.* **2018**, *57*, 7136–7145.

(34) Wang, D. T.; Liu, S. H.; Shao, M. F.; Zhao, J. H.; Gu, Y. K.; Li, Q. Y.; Zhang, X. X.; Zhao, J. S.; Fang, Y. Z. Design of SnO₂ Aggregate/Nanosheet Composite Structures Based on Function-Matching Strategy for Enhanced Dye-Sensitized Solar Cell Performance. *Materials* **2018**, *11*, No. 1774.

(35) Li, G. C.; Li, Y. P.; Lin, G. N.; Wang, D.; Guo, P.; Li, X. B.; Chung, K. H. Synthesis of unsupported Co-Mo hydrodesulfurization catalysts with ethanol-water mixed solvent: Effects of the ethanol/water ratio on active phase composition, morphology and activity. *Appl. Catal., A* **2020**, *602*, No. 117663.

(36) Gayathri, R.; Rajeswaran, P.; Raja, G.; Bavaji, S. R.; Ameen, N.; Shkir, M. Fabrication of WO₃ nanotubes/graphene oxide nanosheets hybrid structures: Enhanced solar conversion efficiency in dye sensitized solar cell. *Diamond Relat. Mater.* **2021**, *119*, No. 108562.

(37) Lu, X. H.; Zheng, Y. Z.; Bi, S. Q.; Wang, Y.; Tao, X.; Dai, L. M.; Chen, J. F. Multidimensional ZnO Architecture for Dye-Sensitized Solar Cells with High-Efficiency up to 7.35%. *Adv. Energy Mater.* **2014**, *4*, No. 1301802.

(38) Xu, L. B.; Xu, J.; H, H. H.; Cui, C.; Ding, Z. X.; Yan, Y. M.; Lin, P.; Wang, P. Hierarchical submicroflowers assembled from ultrathin anatase TiO₂ nanosheets as light scattering centers in TiO₂ photoanodes for dye-sensitized solar cells. *J. Alloys Compd.* **2019**, *776*, 1002–1008.

(39) Xu, X. Q.; Qiao, F. J.; Dang, L. Y.; Lu, Q. Y.; Gao, F. Porous Tin Oxide Nanosheets with Enhanced Conversion Efficiency as Dye-Sensitized Solar Cell Electrode. *J. Phys. Chem. C* **2014**, *118*, 16856–16862.

(40) Ghaithan, H. M.; Qaid, S.; Hezam, M.; Labis, J. P.; Alduraibi, M.; Bedja, I. M.; Aldwayyan, A. S. Laser induced photocurrent and photovoltage transient measurements of dye-sensitized solar cells based on TiO₂ nanosheets and TiO₂ nanoparticles. *Electrochim. Acta* **2016**, *212*, 992–997.

(41) Zheng, Y. Z.; Ding, H. Y.; Liu, Y.; Tao, X.; Cao, G. Z.; Chen, J. F. In situ hydrothermal growth of hierarchical ZnO nanourchin for high-efficiency dye-sensitized solar cells. *J. Power Sources* **2014**, *254*, 153–160.

(42) Feng, C. Q.; Li, Y. R.; Wang, M.; Zhao, G. Y.; Wang, Z. S. Self-assembly of cobalt sulfide nanosheets into nanoflowers and ordered nanosheets arrays for dye-sensitized solar cells. *Electrochim. Acta* **2019**, *301*, 220–228.

(43) Ahn, S. H.; Kim, D. J.; Chi, W. S.; Kim, J. H. One-dimensional hierarchical nanostructures of TiO₂ nanosheets on SnO₂ nanotubes for high efficiency solid-state dye-sensitized solar cells. *Adv. Mater.* **2013**, *25*, 4893–4897.

(44) Peng, J. D.; Wu, Y. T.; Yeh, M. H.; Kuo, F. Y.; Vittal, R.; Ho, K. C. Transparent Cobalt Selenide/Graphene Counter Electrode for Efficient Dye-Sensitized Solar Cells with Co²⁺/3⁺-Based Redox Couple. *ACS Appl. Mater. Interfaces* **2020**, *12* (40), 44597–44607.

(45) Koo, B. R.; Oh, D. Y.; Riu, D. H.; Ahn, H. J. Improvement of Transparent Conducting Performance on Oxygen-Activated Fluorine-Doped Tin Oxide Electrodes Formed by Horizontal Ultrasonic Spray Pyrolysis Deposition. *ACS Appl. Mater. Interfaces* **2017**, *9* (51), 44584–44592.

(46) Zambrzycki, M.; Piech, R.; Raga, S. R.; Lira-Cantu, M.; Fraczek-Szczypta, A. Hierarchical carbon nanofibers/carbon nanotubes/NiCo nanocomposites as novel highly effective counter electrode for dye-sensitized solar cells: A structure-electrocatalytic activity relationship study. *Carbon* **2023**, *203*, 97–110.

(47) Gao, R.; Tian, J. J.; Liang, Z. Q.; Zhang, Q. F.; Wang, L. D.; Cao, G. Z. Nanorod–nanosheet hierarchically structured ZnO crystals on zinc foil as flexible photoanodes for dye-sensitized solar cells. *Nanoscale* **2013**, *5*, 1894–1901.

(48) Tian, J. J.; Uchaker, E.; Zhang, Q. F.; Cao, G. Z. Hierarchically structured ZnO nanorods–nanosheets for improved quantum-dot-sensitized solar cells. *ACS Appl. Mater. Interfaces* **2014**, *6*, 4466–4472.